

Project: B8_01 - Monitoring aerosols above clouds

Author: Matthew Jennings, Candidate Number: 1032903

Supervisors: Dr A. C. Povey, Prof R. G. Grainger

Abstract

Reliably determining cloud properties with satellites is of immense importance for climate forecasts because clouds significantly moderate planetary energy budget and weather. In this study, radiative transfer simulations are performed to investigate how cloud property measurements may be affected by the presence of an overlying aerosol. A simple atmospheric model is developed, and an algorithm is produced to determine the impact of aerosols on measurements of cloud effective radii (CER) and cloud optical depth (COD). These methods are applied to three physically interesting locations with realistic model properties. Results suggest that aerosols typically increase top-of-atmosphere intensity in visible wavelengths and induce a wide range of bias errors on both CER and COD which are not straightforward to account for.

1. Introduction

Accurately determined cloud properties are important input for weather forecasts and climate prediction. Clouds play an important and complex role in the earth's climate through the planetary radiation budget, transport of heat/moisture and precipitation [1]. Two key parameters which characterise cloud influence are COD and CER.

COD can be thought of as a macroscopic measure of cloud 'transparency' and can be defined as:

$$\tau^c = \ln\left(\frac{\Phi^i}{\Phi^t}\right)$$

where Φ^i and Φ^t are the incident and transmitted radiant fluxes received by the cloud along the line of sight. Typically, clouds with $\tau^c \gg 1$ are visibly opaque.

Because clouds are generally more reflective than the surface, they contribute heavily (around two thirds) to the planetary albedo to cool the surface [2]. This cooling is offset by a blanketing effect whereby clouds reradiate infrared (IR) radiation emitted from the surface [3]. COD plays a crucial role in this energy balance [4].

Within a cloud, individual droplet diameters vary in size. Typical liquid cloud particles have a radius around 14 μm [5].

CER is defined as the ratio of the third moment of the droplet size distribution, $n(r)$, to the second moment:

$$r^c = \frac{\int_{-\infty}^{\infty} r^3 \cdot n(r) dr}{\int_{-\infty}^{\infty} r^2 \cdot n(r) dr}$$

and is a central property of cloud microphysics.

Cloud droplets may form via homogenous or heterogenous condensation and proceed to grow through coalescence of liquid droplets or freezing to ice crystals. Above a certain size, these droplets may fall to the ground as precipitation. Cloud droplet size is a fundamental characteristic of rain microphysical processes, with existing research showing that variations in CER can lead to dramatic variation in the dynamics of rain formation [6, 7].

Accurate determination of COD and CER on a global scale is therefore of immense importance in producing climate models to reliably forecast planetary temperature trends and weather. Such mapping is achieved via remote sensing with satellites to collect data. Statistical determination of cloud properties from this data is referred to as 'cloud retrieval'. A proven practical and effective method to retrieve COD and CER is through measuring top of atmosphere (TOA) spectral radiant intensity, I_λ .

Unfortunately, the accuracy of this method depends on atmospheric conditions. Furthermore, even small variations in TOA intensity can lead to large uncertainties in retrieved COD and CER [8]. Whilst some sources of uncertainty are well understood,

one factor which has been widely omitted from most retrieval algorithms is the impact of aerosols above cloud (AAC).

Aerosols in this context are fine solid or liquid particles suspended in the atmosphere. Examples include dust from windswept deserts, haze from urban pollution and sea spray from breaking waves.

The scattering and absorption effects of overlying aerosol layers have been neglected from most satellite cloud retrievals approaches, including widely used products such as the Moderate resolution Imaging Spectrometer (MODIS) [9]. This is because the optical depth of AAC is assumed to be much smaller than the COD, and the aerosol’s optical properties are usually unknown.

However, existing research argues that there is a significant difference between clean and aerosol-laden clouds [10]. In the specific case of the SE Atlantic, Meyer et al. [11] found that the presence of smoke from biomass burning introduced positive bias errors in measurements of the CER and COD of 2% and 9% respectively.

Finally, retrieved cloud properties are often used in climate models to determine other important quantities such as surface temperature and aerosol properties. Measurements of surface temperature are used to guide action on climate change, and aerosol has been cited as the single largest source of uncertainty on the planetary radiation budget [12]. Retrieval errors on COD and CER can result in mis-determination of these vital quantities.

A better understanding of the impact of aerosols on retrieved cloud properties is therefore essential in removing bias errors and thus improve forecasts of global climate. This study outlines a method for estimating the induced bias errors on the retrieved CER and COD in the presence of overlying aerosol using radiative transfer simulations.

Sections 2.1, 2.2 describe the atmospheric model used for calculations. Three physically interesting case study locations are modelled with realistic properties given in Section 2.3. The algorithm used for cloud retrieval and determining aerosol-induced error is outlined in Sections 2.4, 2.5. Methods are applied to the chosen locations, with results and limitations discussed in Sections 3, 4.

2. Methods

2.1 Radiative Transfer Calculations

Solar radiation incident on the earth undergoes interactions with the atmosphere and surface before arriving at satellites. By measuring the TOA spectral radiant intensity, I_λ , we hope to infer the interactions which have taken place and determine atmospheric properties.

For this report, the zenith is taken at the vertical with $(\theta, \phi)_{zenith} = 0$ and the resulting radiation is observed at an angle (ϕ_0, θ_0) as shown in Figure 1.

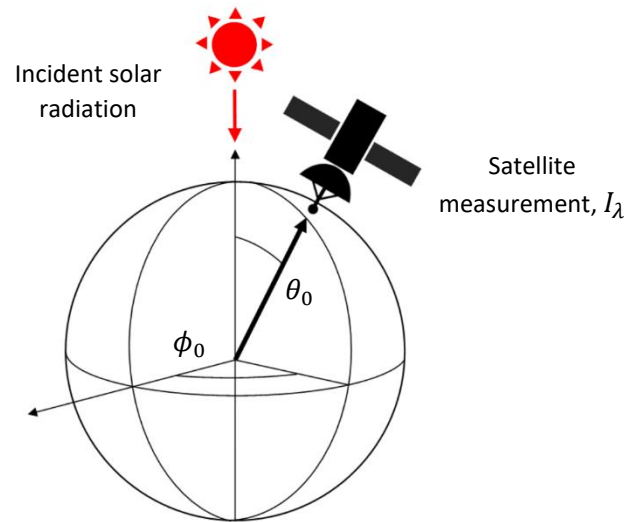


Figure 1: Viewing geometry with the zenith at the vertical. Satellite measures TOA spectral radiant intensity, I_λ .

Radiative transfer describes the propagation of energy through the atmosphere. A beam of light viewed at some angle may have its intensity increased by emission and decreased by absorption or scattering out of the line of sight. Absorption and scattering are together referred to as ‘extinction’.

The emission and extinction from particles can be described by three spectral properties:

- Optical Depth, τ (p1)

As described in Section 1, this encapsulates the extinction of radiation through a material.

- Single scattering albedo, ω_0 (p2)

This measures the fraction of extinction from scattering.

- Scattering phase function, $P(\theta)$ (p3)

This describes the distribution of the scattering direction θ (relative to the incident beam) [13]. It is generally dependent on the size and shape of the particle.

Together, (p2) and (p3) describe scattering, from which the effective radius is inferred. In this report, reflection from the surface is assumed isotropic and determined via the surface albedo:

- Surface Albedo, A^s (p4)

Note that generally (p1-4) are spectral quantities that depend on the observed wavelength, λ . The resulting observed TOA spectral intensity, I_λ , is governed by the ‘radiative transfer equation’. The radiative transfer equation in the atmosphere is highly non-linear. Here, existing numerical methods are used to solve it using simplified models of atmospheric composition and structure.

There are many radiative transfer codes available to solve the radiative transfer equation. This project makes use of the Discrete Ordinates Radiative Transfer Program for a Multi-Layered Plane-Parallel Medium (DISORT) radiative transfer code. Discrete Ordinance refers to the division of the continuum into a discrete number of streams over which to perform calculations. DISORT models monochromatic unpolarized radiative transfer in non-isothermal, vertically inhomogeneous, but horizontally homogeneous media [14].

DISORT was originally written in FORTRAN in 1988 and is used widely for radiative transfer simulations due to its high accuracy and reliability in a range of cases. Alternatives may be computationally faster, whilst the original developers of DISORT comment that “no shortcuts were taken in which accuracy was sacrificed for speed” ([14], p.12).

Unfortunately, DISORT remains largely inaccessible to scientists using more conventional modern programming languages. Therefore, part of this project was dedicated to producing a new Python 3 wrapper to enable the calling of DISORT’s routines. This was packaged and made public under the title ‘py3DISORT’ for the benefit of others pursuing similar research [Appendix B].

2.2 Modelling the atmosphere

Under DISORT’s construction we model the atmosphere with a series of horizontally uniform layers, with each layer having the properties (p1-3). Computationally, we express the phase function (p3) as an expansion in phase moments x_l by:

$$P(\cos\theta) = \sum_{l=0}^N (2l + 1)x_l P_l(\cos\theta) \quad (\text{eq2.1})$$

where P_l are the Legendre Polynomials, normalised such that $x_0 = 1.0$.

All properties are determined at a desired wavelength with an underlying surface specified by (p4). Figure 2 shows a representation of the model used for the simple case of cloud with overlying aerosol. Simulations return I_λ at the given geometry.

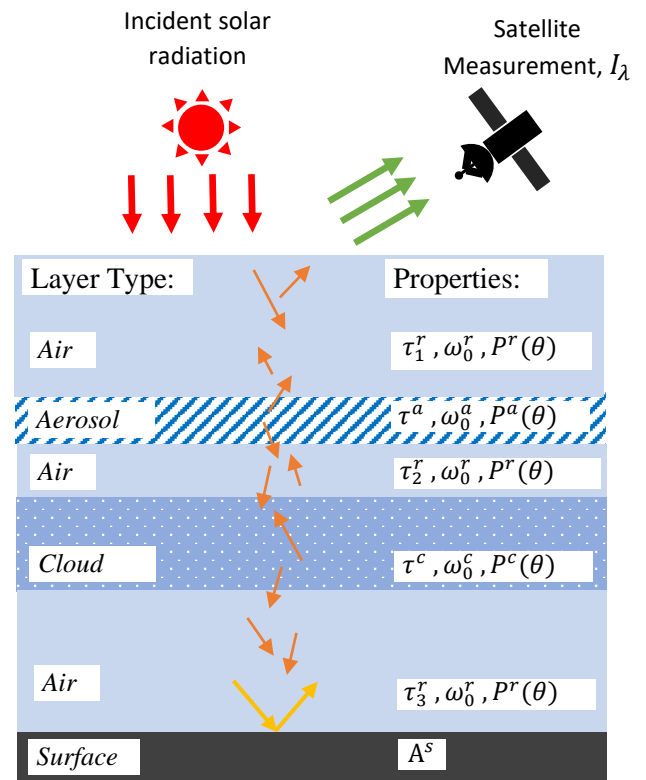


Figure 2: Representation of the model used for radiative transfer simulations in the case of aerosol above cloud. The atmosphere is divided into uniform layers with properties described in Section 2.1.

The model used included the following assumptions:

- Sunlight is incident perpendicular to the underlying surface with $(\theta, \phi)_{zenith} = 0$.
- The underlying surface is assumed to be Lambertian, meaning it has isotropic reflection as determined by $(p4)$.
- The atmosphere includes a uniformly distributed cloud layer of vertical extent 1.0 km, with a cloud top height (CTH) h^c and COD τ^c .
- A uniformly distributed aerosol layer of vertical extent 0.5km lies 0.5km above the cloud, with aerosol top height h^a and AOD τ^a .

These thicknesses were chosen from an in-depth study into the vertical extent of aerosol and cloud layers during overlap events [15]. This study found that cloud-aerosol gaps between 0.1km-1km occur in 45-60% of cases globally, and aerosol layers are < 1km thick in 70-80% of cases. Cloud layer geometry depends heavily on the type of cloud, so a value of 1km was chosen to be consistent with ranges in other studies.

Many cloud and aerosol vertical profiles are used in existing models. A common example is an exponential decay in aerosol optical depth with height [16]. Research shows very low sensitivity of TOA intensity to cloud and aerosol vertical structure; optical depth and effective radii are far more significant [10]. Hence, uniform distributions are assumed in this report for simplicity.

- The cloud phase is taken as liquid water, with CER described by ω_0^c and $P^c(\theta)$.

This was the chosen project scope since absorbing aerosols above ice-phase clouds are less likely [10]. Further, ice cloud contributes less to global cloud cover than liquid cloud and the cloud top heights considered in this study all fall in the troposphere, which contains around 99% of the atmosphere's water vapour [17].

- The overlying aerosol layer is assumed to consist of a single aerosol type with aerosol AER described by ω_0^a and $P^a(\theta)$.

- Molecular Rayleigh scattering is the dominant scattering process in air layers free from aerosol and cloud.

The Rayleigh scattering phase function is:

$$P^r(\theta) = \frac{3}{4}(1 + \cos^2\theta) \quad (eq2.2)$$

which is decomposed as $x_0 = 1.0$ and $x_1 = 0.1$ from $(eq2.3)$.

And the Rayleigh single scatter albedo is taken as $\omega_0^r = 1.0$.

For a surface pressure p_s the Rayleigh optical depth, τ^r of a layer with upper pressure p_u and lower pressure p_l , is calculated from:

$$\tau_i^r = \frac{p_l - p_u}{p_s} \tau_0^r \quad (eq2.3)$$

where τ_0^r is a 'base' Rayleigh depth

$$\tau_0^r = \frac{p_s / 1013.0}{117.03 \lambda^4 - 1.1316\lambda^2} \quad (eq2.4)$$

the pressure at a height z km was found from the hydrostatic equation:

$$p(z) = p_s e^{-\frac{z}{7.0}} \quad (eq2.5)$$

In cloud and aerosol layers the Mie scattering from the larger particles is also accompanied by Rayleigh scattering. The combined optical properties are then calculated from weighted sums of the individual layer properties. An illustrative example for a cloud layer is listed in [Appendix C].

This approach of introducing Rayleigh scattering $(eq2.2-2.5)$ is taken from existing atmospheric models such as the Optimal Retrieval of Aerosol and Cloud (ORAC) algorithm [18].

- Experimentation showed negligible impact of surface pressure variation on total τ and so was taken as a constant $p_s = 1010$ hPa.
- We neglect scattering and absorption of other trace gases, and blackbody emission as governed by the Planck function is taken as negligible at our wavelengths of interest ($\lambda = 0.55\mu\text{m}, 1.6\mu\text{m}$).
- The resulting TOA intensity is taken at viewing geometry of $\theta_0 = 45.0^\circ$ and $\phi_0 = 0.0^\circ$.

2.3 Model parameters

The aim was to apply this model to test algorithms in a range of physically interesting conditions with realistic atmospheric properties. This was achieved by selecting three reference locations and exploring satellite datasets to determine their atmospheric parameters.

2.3.1 Data Collection

The chosen dataset comes from the European Space Agency's cloud Climate Change Initiative (CCI) [19]. Data is sourced from the AATSR (Advanced Along-Track Scanning Radiometer) satellite and provides monthly averages of atmospheric properties. Cloud and surface conditions are provided at a 0.5 x 0.5 latitude x longitude grid resolution. Aerosol properties are determined using the ORAC algorithm [18] and provided in separate datasets at a 1 x 1 latitude x longitude grid resolution.

Averages were taken from the 2011 dataset over each three-month quarter (starting January) to give a recent and complete representation of global atmospheric parameters. More recent data products are available from alternative sensors but give similar results.

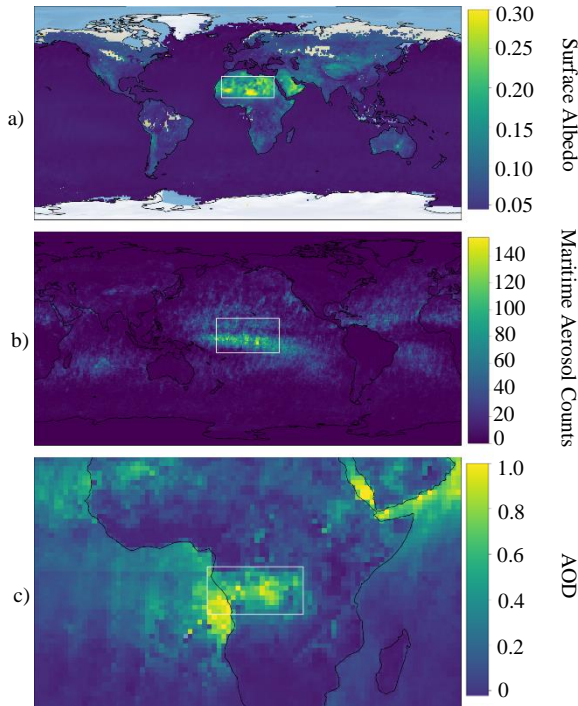
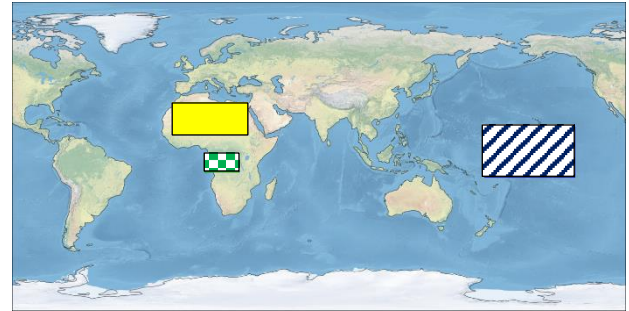


Figure 3: Preliminary exploration of a) Surface Albedo, b) Maritime Aerosol Counts and c) Aerosol Optical Depth. Data shown at $\lambda = 0.55\mu\text{m}$.

To identify physically interesting locations with varied and relevant aerosol regimes, a preliminary exploration of optical properties was performed. Figure 3 shows global distributions of surface reflectance, aerosol type, and AOD. This guided the selection of three reference locations which are shown in Figure 4.



Location Name	Latitude (°N)	Longitude (°E)	Quarter
a) Sahara	[13,31]	[-11,33]	2011 Q1
b) Pacific	[-12,17]	[172,225]	2011 Q1
c) Congo	[-9,1]	[8,28]	2011 Q3

Figure 4: Final reference location choices. Regions chosen for their different and climatically relevant aerosol regimes.

The Sahara was chosen for its uniquely high surface reflectivity (Fig 3a) and strong presence of dust aerosol.

The Pacific region has constantly low surface reflectivity (Fig 3a), and strong prevalence of Maritime aerosol (Fig 3b).

The Congo was picked for its anomalously high AOD (Fig 3c) in the summer to explore impacts of optically thick aerosol layers.

2.3.2 Parameter Estimates

Examining the datasets allowed determination of typical values for the aerosol optical depth (AOD) and aerosol effective radii (AER), cloud top height (CTH) and Surface Albedo. These properties were estimated from an average over all box pixels (for which data was collected) for the chosen quarter.

ORAC [18] classifies aerosols into 10 discrete types which vary in composition (e.g: dust, smoke, sea salt) and optical properties. The total AOD was assumed to arise from the dominant aerosol present over the region.

The dominant aerosol type was selected from a review of the ‘aerosol type counts’ dataset variable. Discussions were also held with the developers of the ORAC retrieval with experience in global aerosol distributions and the limitations of the retrieval methods. The large AOD over the Congo (Fig 3c) was attributed to biomass burning. Once the aerosol type was decided, the aerosol’s optical properties were provided by the creators of ORAC. This specified single scatter albedo ω_0^a and

corresponding scattering phase function $P^a(\theta)$ of the overlying layer at the mean AER.

The ω_0^c and $P^c(\theta)$ of the cloud layer at the mean CER were provided from a standard liquid-phase cloud profile in the literature [13]. The atmosphere in each reference location was now fully specified. A summary of the values obtained is listed in Figure 5.

Parameter	Sahara Region	Pacific Region	Congo Region
Aerosol Optical Depth, τ_λ^a ($\lambda = 0.55\mu\text{m}$)	0.242	0.117	0.549
Aerosol Optical Depth, τ_λ^a ($\lambda = 1.6\mu\text{m}$)	0.153	0.089	0.269
Aerosol Effective Radii, r^a (μm)	0.5	0.5	0.5
Surface Albedo A_λ^s ($\lambda = 0.55\mu\text{m}$)	0.180	0.029	0.076
Surface Albedo A_λ^s ($\lambda = 1.6\mu\text{m}$)	0.412	0.020	0.144
Cloud Top Height, h^c (Km)	4.81	6.03	5.58
Aerosol Type ‘Name’ (ORAC-AATSR Model) [20]	‘Dusty Maritime’ (A76)	‘Maritime’ (A77)	‘Biomass Smoke’ (A79)

Figure 5: Final (spectral) model parameters used for radiative transfer simulations. The values are obtained from pixel averages for the regions as described in Sections 2.3.1, 2.3.2. A full visual representation is given in [Appendix A]. Aerosol Effective Radii $r^a = 0.5\mu\text{m}$ was the closest match with provided data for ω_0^a , $P^a(\theta)$ at $\lambda = 0.55\mu\text{m}$, $1.6\mu\text{m}$ as discussed in Section 2.3.2. The high precision listed is for reproducibility of results – values are a rough realistic estimate of region properties.

2.4 Algorithm to model Cloud retrieval

Cloud retrieval refers to the process of determining cloud optical properties via remote sensing. The first known example of a modern cloud retrieval is widely considered to be Nakajima and King [20], with similar methods still used today. These retrievals use a ‘hatch diagram’ to simultaneously determine COD, τ^c and CER, r^c from TOA intensity measurements at two wavelengths (for example, Fig.6). τ^c and r^c are assumed to be dominantly sensitive in the visible $\lambda = 0.55\mu\text{m}$ and IR $\lambda = 1.60\mu\text{m}$ respectively. The wavelengths chosen are common instrumental channels used for such retrievals.

Radiative transfer simulations are performed under a wide range of cloud conditions, with all other atmospheric parameters fixed. Satellite intensity measurements are compared to these predetermined values to retrieve the cloud properties. The TOA

spectral radiant intensity, I_λ , is normalized over a hemisphere and divided by the incident solar flux to give a Reflection Function, R_λ . Under viewing geometry used (Fig.1) and selecting units such that the solar flux is 1.0, this is simply:

$$R_\lambda = \pi I_\lambda \quad (\text{eq2.6})$$

This method may fail for $\tau^c \lesssim 10$ and $r^c \lesssim 8 \mu\text{m}$ due to line overlap leading to ambiguity as documented in study [20] and seen in Fig.6a.

For the retrieval of COD and CER measurements between the predetermined values, two bilinear interpolations are performed to give the result. For an illustrative example, a measurement at the red X in Fig.6a would correspond to $\tau^c \approx 18$ and $r^c \approx 10 \mu\text{m}$.

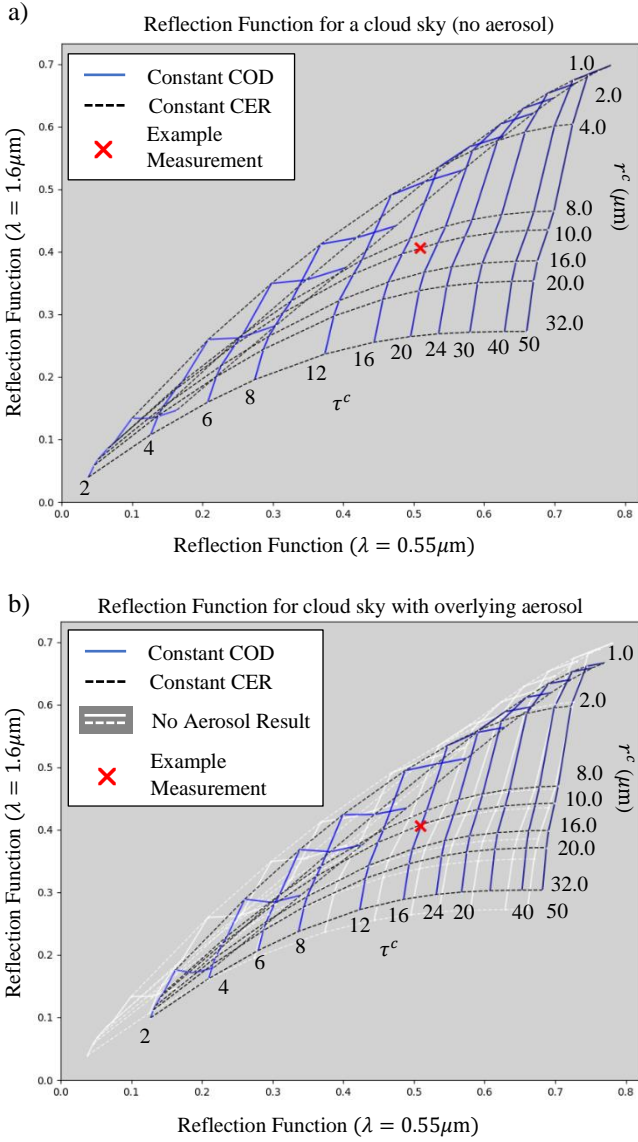


Figure 6: Hatch diagram method of cloud retrieval a) for a clouded sky without aerosol and b) for an overlying aerosol above cloud. X shows an example satellite measurement to illustrate the bias error in values for COD and CER in the presence of aerosol.

We seek to examine the effects of aerosol above cloud on such hatch diagrams, which serve here as a representation of a general cloud retrieval.

2.5 Algorithm to determine retrieval error

Radiative transfer calculations are repeated in the presence of overlying aerosol layer (with properties determined by the methods in 2.3.2). This perturbs the hatch diagram as shown in Fig.6b.

For a given satellite measurement, the methods of section 2.3 are used to retrieve the COD, τ^c and CER, r^c under the assumption of a clean sky (Fig 6a). The retrieved values are compared to the “true”

values obtained from considering the effect of an overlying aerosol (Fig 6b). This gives an absolute error on our retrieval at a given retrieved COD and CER due to neglecting the aerosol layer in the retrieval. For an illustrative example, if an aerosol were indeed present for the sky for Fig.5a, the true values at the red X would be to $\tau^c \approx 16$ and $r^c \approx 10 \mu\text{m}$. There would be positive bias in the original measurement ($\tau^c \approx 18$) of $\Delta\tau^c \approx 2$.

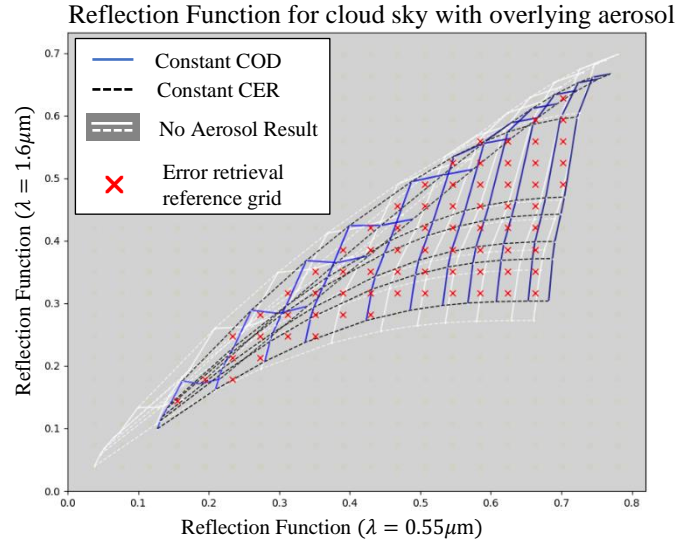


Figure 7: Illustration of COD and CER error estimation algorithm. The methods of Section 2.3 are applied to retrieve COD and CER with and without the presence of aerosol at reference values. Retrievals are compared to give the error from aerosol.

This error is calculated for a reference grid of CER and COD points within the overlapping domains of the individual hatch diagrams (Fig.7). To estimate the errors or values of the CER, COD between our grid points, a Clough-Tocher interpolation is performed [21]. Here, this is a generalisation of cubic interpolation to 3 dimensions. This algorithm was chosen both for its efficiency and ability to show smooth local trends that may exist in our data, which other approaches such as Nearest Neighbour and Barycentric interpolation lack.

The number of reference interpolation points was a trade-off between program efficiency and potential accuracy. The result is a list of values for the bias errors (caused by the presence of aerosol above cloud) on the CER, Δr^c and COD, $\Delta\tau^c$ for any (r^c, τ^c) retrieved under the assumption of a clean sky. This algorithm is applied to each of the three reference locations, to provide an indication of bias errors which may be present in cloud retrievals at these areas. Results are shown in Section 3.

3 Results

3.1 Pacific Region

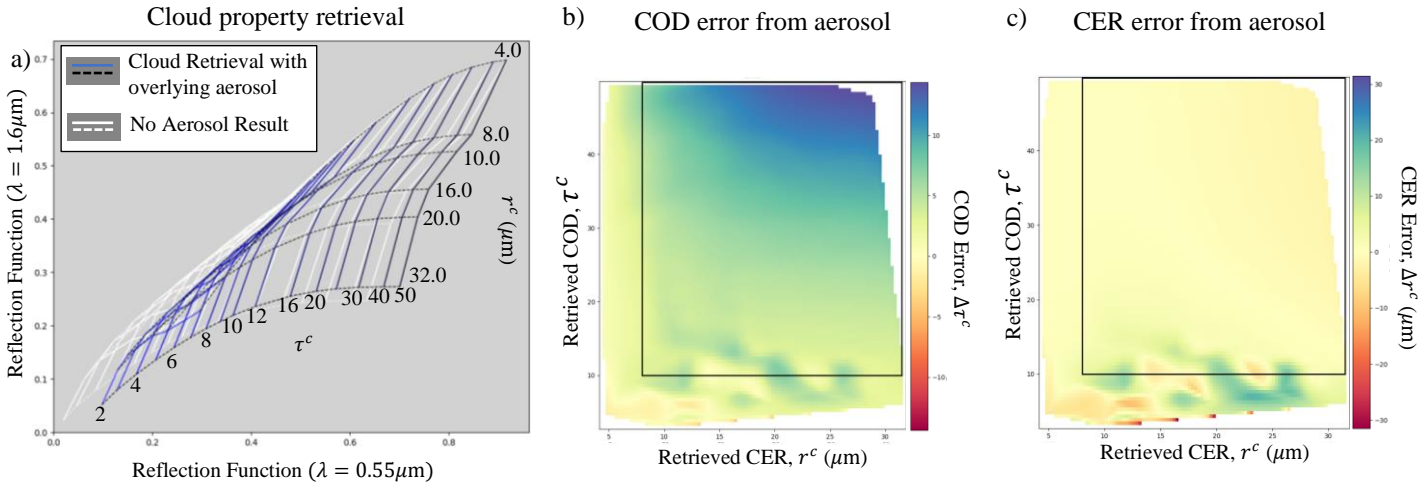


Figure 8: Results for the Pacific Region described in Section 2.3.1. a) Hatch Diagram cloud retrieval performed with and without the presence of an overlying aerosol. b), c) Estimated induced bias error from aerosol on the COD, CER obtained from the Methods in Section 2.5. Box indicates the range of values for which the cloud retrieval is considered valid.

The relationship of TOA intensity in the Visible and IR wavelengths (as in Fig.9a) closely matches the asymptotic behaviour described in [9]. Successfully reproducing such hatch diagrams indicates that the Python wrapper written for calling the DISORT radiative transfer code could be used as an effective tool for future researchers.

The Pacific region shows that overlying aerosol tends to increase TOA intensity in the visible at $\lambda = 0.55\mu\text{m}$ (Fig.9a). The net change of the IR signal transitions between positive and negative in different cloud conditions. Such transitioning has also been found in another existing study examining

hatch diagrams for aerosol above cloud [9]. The range of valid cloud retrieval falls within the boxes drawn in Fig.8a,8b. This was done to minimise interpolation ambiguity as discussed in Section 2.4. The interquartile mean (IQM) over this range is used to indicate errors. This reduces the impact of outlying values. In Fig.8b and Fig.8c there is a IQM bias error on the COD of $\Delta\tau^c \sim 22.0\%$ and on the CER of $\Delta r^c \sim 0.2\%$. This suggests the impact of maritime aerosol on the CER is negligible in retrievals over the Pacific, indeed dotted lines in (Fig.9a) are near unaltered by the aerosol. COD may be subject to positive bias errors.

3.2 Congo Region

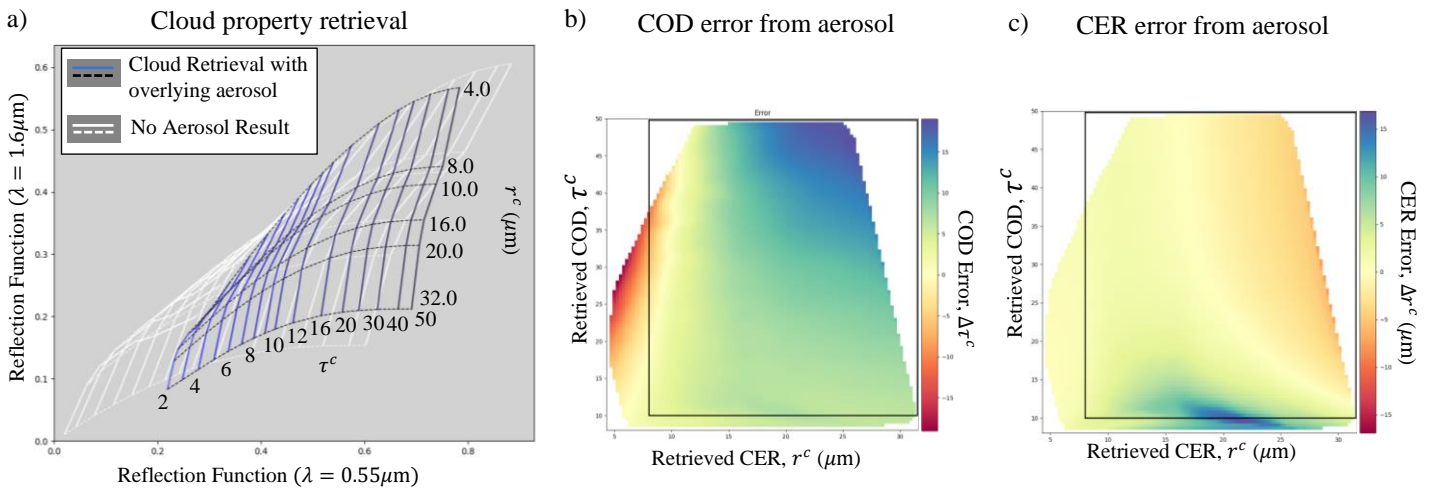


Figure 9: Same as Figure 8, with results for the Congo Region described in Section 2.3.1

The Congo region was selected for its large aerosol optical depth. The effect of this is evident in Fig.10a which shows significant deviation of the plot in the presence of smoke aerosol (compared, for example, to Fig.9a). Results indicate an IQM positive bias

error on the COD of $\Delta\tau^c \sim 29.6\%$ and on the CER of $\Delta r^c \sim 6.7\%$ (Fig.9b,9c). These results are somewhat consistent with [11] which also found positive bias errors on both COD and CER over the SE Atlantic, but of 9% and 2% respectively.

3.3 Sahara Region

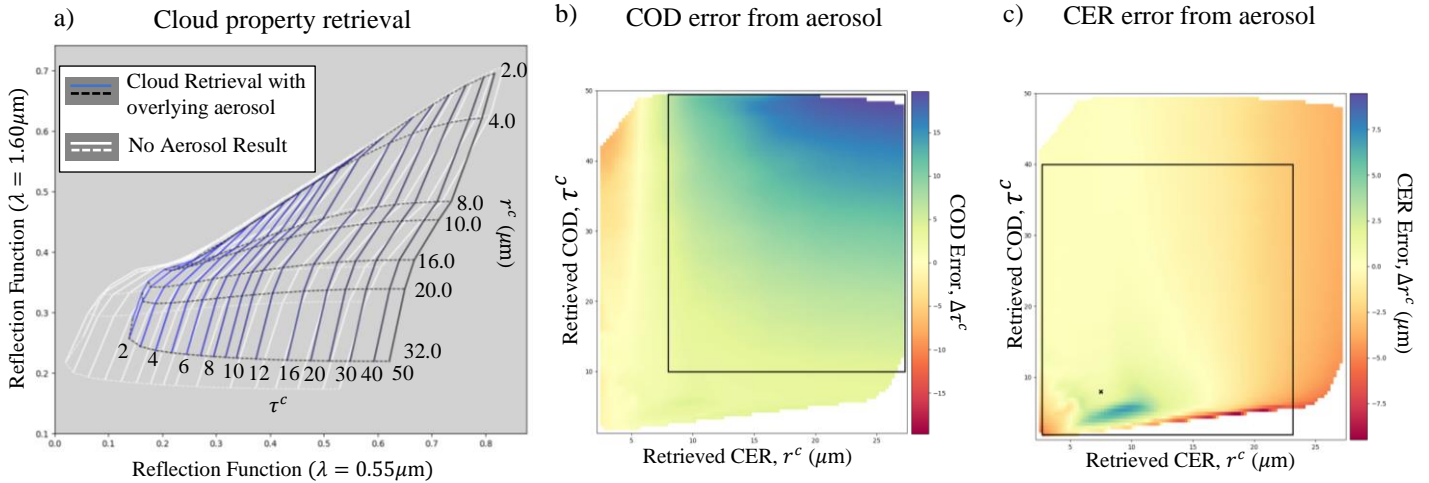


Figure 10: Same as Figures 8,9, with results for the Congo Region described in Section 2.3.1

In the Sahara location, the TOA signal in the IR range is notably larger than the other regions (note the vertical scale which starts at 0.1). This may be attributed to the high surface reflectance of the underlying desert at this thermal wavelength. Aerosol has the general effect of increasing both IR and visible spectral intensity. This increase is more pronounced for larger radii and lower optical

depths. Here the presence of aerosol seems to give a general underestimate of the CER and overestimate of COD (Fig.8b,8c). Results again indicate a IQM positive bias error on the COD of $\Delta\tau^c \sim 29.5\%$ (Fig.9b). The bias error on the CER is now negative and found to be $\Delta r^c \sim -4.9\%$ (Fig.9c).

3.4 Comments

All regions suggest that the typical effect of aerosol in common cloud conditions is to increase the TOA intensity in the visible $\lambda = 0.55 \mu\text{m}$. This generally results in an overestimate of COD. The fractional impact is consistently larger for smaller values of COD (Fig.8a,9a,10a). Retrievals at very low $\tau^c \lesssim 10$ and $r^c \lesssim 8 \mu\text{m}$ fall outside the range our retrievals are valid (as discusses in Section 2.4) and are not explored. Results from all regions indicate that overlying aerosol can lead to significant changes in TOA measurements. The magnitude (and even sign) of aerosol-induced bias errors for these simple cloud retrievals are dependent on the precise cloud and surface conditions.

The accuracy for intensity calculations using DISORT is quoted to be $< 1\%$ at the computational precision used [14]. Typical TOA satellite measurements experience a minimum instrumental uncertainty of $\sim 2\%$. This arises from various factors such as spectral dependence. The intensity values plotted in (Fig.8a,9a,10a) were therefore considered a true reflection of the model conditions.

However, there was inevitable ambiguity in the 'retrieved' values for the CER and COD when using interpolation methods. This caused outliers to be present in the data, particularly near overlapping domain edges. This may have resulted in larger perceived errors from aerosol which in fact arise from errors in determining the cloud properties.

The worst-case bias errors in COD and CER of 29.6% and 6.7% are around a factor of three larger than existing research, possibly because of this error. Attempts were made to resolve this issue by considering the IQM only, and by performing radiative transfer calculations for intermediate values of COD. It was found that a higher resolution of the scattering properties at intermediate CER would also be needed. This limits the validity of the specific error estimates found.

4 Conclusions

The presence of aerosols above cloud can lead to bias errors on satellite measurements of CER and COD which are properties of immense importance for reliable climate forecasts. Radiative transfer calculations were performed to examine TOA intensity measurements for a simple model of cloud with and without an overlying aerosol layer. Realistic model properties were determined for three physically interesting locations using past satellite datasets. A preliminary algorithm was developed to determine the impact of the aerosol on retrieved CER and COD and applied at the three reference locations.

Results indicate the typical effect of aerosol is to increase the TOA intensity in the visible $\lambda = 0.55\mu\text{m}$. This generally results in an overestimate of COD, and the impact is consistently larger for smaller values of COD. The error algorithm used suggests that cloud retrievals over the Pacific may have positive bias errors for the COD and CER of $\Delta\tau^c \sim 22.0\%$ and $\Delta r^c \sim 0.2\%$ respectively. Biomass burning in the Congo was found to result in positive bias errors as high as $\Delta\tau^c \sim 29.6\%$ $\Delta r^c \sim 6.7\%$. With its high underlying surface albedo,

Nonetheless, these results confidently display that aerosols can have a significant impact on retrieved cloud properties. This preliminary study highlights the challenges of obtaining exact estimates of error from aerosol without access to advanced cloud retrieval algorithms. Focusing on the specific values given above is therefore not necessarily useful. Much more interesting is the presence, range, and inconsistency of these bias errors. Results provide strong evidence that aerosols can impact TOA measurements, and the error on retrieved cloud properties is not easily accounted for.

dusty conditions over the Sahara gave errors of $\Delta\tau^c \sim 29.5\%$ and $\Delta r^c \sim -4.9\%$. The accuracy of precise error values was heavily limited by the basic cloud retrievals possible with available resources. Nonetheless, results suggest strong evidence that aerosols influence TOA measurements of underlying cloud, and that the bias error on retrieved cloud properties is not easily accounted for. These effects should be considered when developing cloud retrieval algorithms in to order to improve climate forecasts.

Further research would be needed to obtain more accurate error estimates. This may be partly achieved with access to a more advanced cloud retrieval algorithm. This may include high resolution radiative transfer calculations and data from more wavelengths. The Python wrapper produced for calling the DISORT radiative transfer code may serve as a useful tool for others. Models could be improved with relaxed assumptions on atmospheric vertical profiles and viewing geometry. In-situ observations could be used to help verify results.

Bibliography

- [1] J.G. Hurley (2008), *Detection and Retrieval of Clouds from MIPAS*, Doctor of Philosophy Thesis, Exeter College, University of Oxford.
- [2] K. E. Trenberth and J. T. Fasullo (2011), *Tracking Earth's Energy: From El Niño to Global Warming*, doi: 10.1007/s10712-011-9150-2, Surveys in Geophysics.
- [3] W.B. Rossow and A.A. Lacis (1990), *Global, seasonal cloud variations from satellite radiance measurements. Part II: Cloud properties and radiative effects*, pp: 1204-1213, doi:10.1175/1520-0442, Journal of Climate.
- [4] E. J. Jensen, S. Kinne and O. B. Toon (1994), *Tropical cirrus cloud radiative forcing: Sensitivity studies*, doi: 10.1029/94GL01358, Geophysical Research Letters.
- [5] R.K. Pachauri, L.A. Meyer and Core Writing Team (2013), *Assessment of global cloud datasets from satellites*, pp: 1031–1049, doi:10.1175/BAMS-D-12-00117.1, Bulletin of the American Meteorological Society.
- [6] P. K. Wang (2013), *Physics and Dynamics of Clouds and Precipitation*, ISBN-10: ISBN-10 1107005566, Cambridge University Press.
- [7] A. Thomas, V.P. Kanawade, K. Chakravarty and A.K. Srivastava (2021) *Characterization of raindrop size distributions and its response to cloud microphysical properties*, doi: 10.1016/j.atmosres.2020.105292, Atmospheric Research.
- [8] S. Zeng, C. Cornet, F. Parol, J. Riedi, and F. Thieuleux (2012), *A better understanding of cloud optical thickness derived from the passive sensors MODIS/AQUA and POLDER/PARASOL in the A-Train constellation*, doi:10.5194/acp-12-11245-2012, EGU Atmospheric Chemistry and Physics.
- [9] J.M.Haywood, S.R.Osborne and S.J.Abel (2003), *The effect of overlying absorbing aerosol layers on remote sensing retrievals of cloud effective radius and cloud optical depth*, doi: 10.1256/qj.03.100, Royal Meteorological Society.
- [10] A. M. Sayer, N.C.Hsu, C.Bettenhausen, J. Lee, J.Redemann, B. Schmid and Y.Shinozuka (2016), *Extending “Deep Blue” aerosol retrieval coverage to cases of absorbing aerosols above clouds: Sensitivity analysis and first case studies*, doi: 10.1002/2015JD024729, Journal of Geophysical Research.
- [11] K. Meyer, S.Platnick and Z.Zhang (2015), *Simultaneously inferring above-cloud absorbing aerosol optical thickness and underlying liquid phase cloud optical and microphysical properties using MODIS*, doi:10.1002/2015JD023128, Journal of Geophysical Research.
- [12] R.K. Pachauri, L.A. Meyer and Core Writing Team, (2014) *Climate Change 2014: Synthesis Report*, IPCC, Geneva, Switzerland.
- [13] J.H.Seinfeld and S.N.Pandis (2016) *Atmospheric Chemistry and Physics*, p: 693, ISBN: 978-1-118-94740-1, Wiley.
- [14] Knut Stamnes, Si-Chee Tsay and Istvan Laszlo (2000) *DISORT, a General-Purpose Fortran Program for Discrete-Ordinate-Method Radiative Transfer in Scattering and Emitting Layered Media: Documentation of Methodology*, In url: https://www.meteo.physik.uni-muenchen.de/~emde/lib/exe/fetch.php?media=teaching:radiative_transfer:disortreport1.1.pdf
- [15] A. Devasthale and M. A. Thomas (2010) *A global survey of aerosol-liquid water cloud overlap based on four years of CALIPSO-CALIOP data* doi:10.5194/acp-11-1143-2011, EGU Atmospheric Chemistry and Physics.
- [16] M. Hess, P. Koepke and I. Schult (1998), *Optical Properties of Aerosols and Clouds: The Software Package OPAC*, doi: 10.1175/1520-0477(1998)079<0831:OPOAAC>2.0.CO;2, American Meteorological Society.
- [17] B.Yi, A.D. Rapp, P.Yang, B.A.Baum and M.D. King (2017) *A comparison of Aqua MODIS ice and liquid water cloud physical and optical properties between collection 6 and collection 5.1: Cloud radiative effects*, doi:10.1002/2016JD025586, Journal of Geophysical Research.

[18] G.E. Thomas et al (2017), *Algorithm Theoretical Basis Document (ATBD) AATSR Oxford-RAL Aerosol and Cloud (ORAC) Version 3.0*, In url: https://climate.esa.int/sites/default/files/Aerosol_cci2_ATBD_ATSR_ORAC_v3.0.pdf, ESA Climate Change Initiative.

[19] ESA cloud Climate Change Initiative (*Cloud_cci*): *AATSR2-AATSR monthly gridded cloud properties, version 3.0*. In url: https://data.ceda.ac.uk/neodc/esacci/cloud/data/version3/L3C/AATSR2-AATSR/v3.0/AATSR_ENVISAT .

[20] T.Nakajima and M.D King (1990), *Determination of the Optical Thickness and Effective Particle Radius of Clouds from Reflected Solar Radiation Measurements*, doi: 10.1175/1520-0469(1990)047<1878:DOTOTA>2.0.CO;2), American Meteorological Society.

[21] G. Farin (1986), *Triangular Bernstein-Bézier patches*, doi: 10.1016/0167-8396(86)90016-6, Computer Aided Geometric Design.

Appendices

A. Model parameter Data

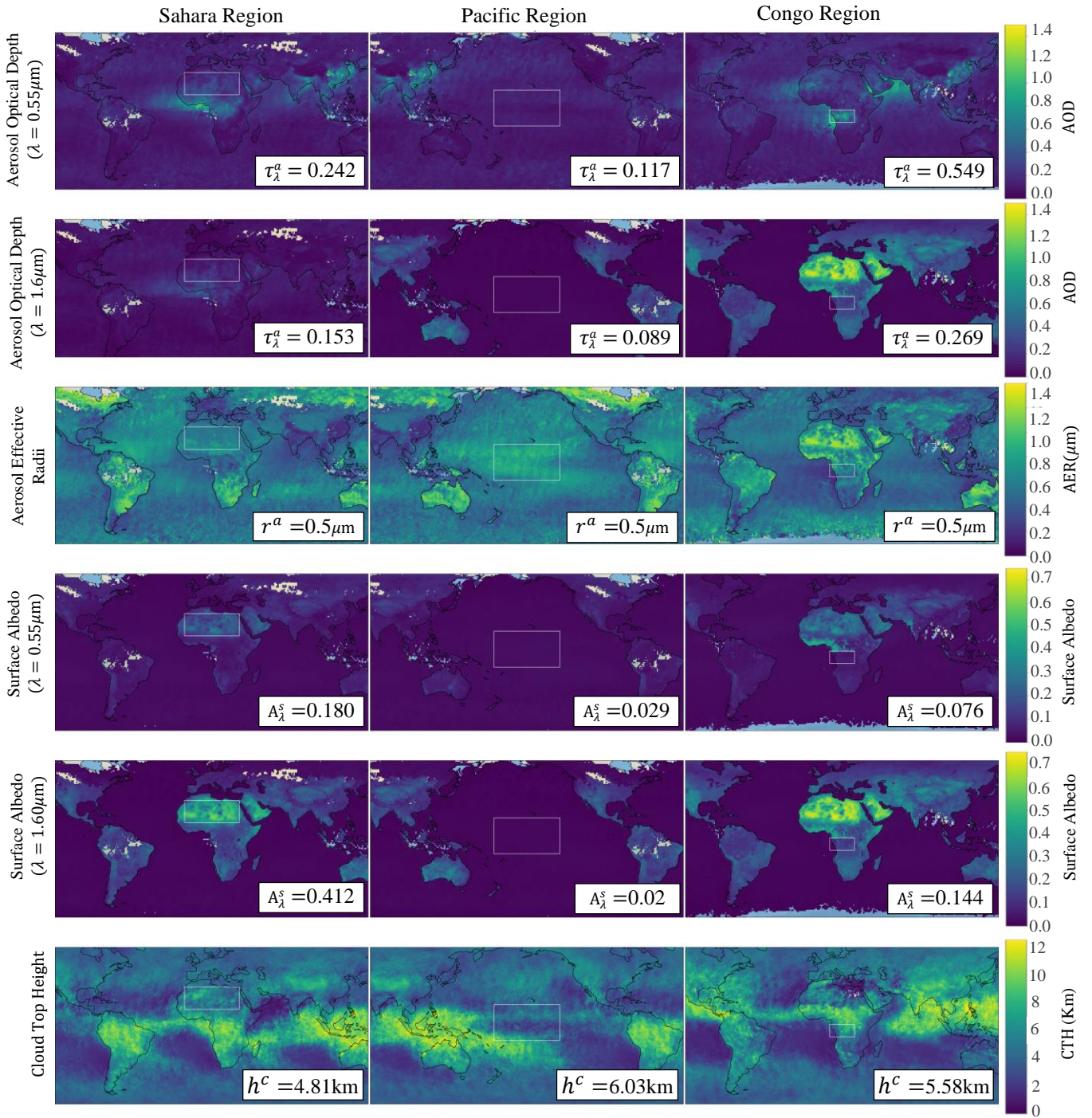


Figure A1: A full visual representation of how the model parameters listed in Figure 7 were obtained. Values shown are the pixel means over the regions and timespans described under Section 2.3.1.

B. Python3 Wrapper for DISORT

To numerically solve the radiative transfer equation, this project makes use of the Discrete Ordinates Radiative Transfer Program for a Multi-Layered Plane-Parallel Medium (DISORT) radiative transfer code [13]. DISORT was originally written in FORTRAN in 1988 and is preferred for its high accuracy and reliability.

Unfortunately, DISORT remains largely inaccessible to scientists using more conventional modern programming languages. Part of this project was dedicated to producing a new Python 3 wrapper to enable the calling of DISORT's routines. This was packaged and made public under the title *'py3DISORT'* for the benefit of others pursuing similar research.

Source code and documentation for this wrapper was made public at the GitHub repository under the title *py3DISORT*.

C. Combining Atmospheric Layers

Consider a combined atmospheric layer containing both cloud Mie scattering and Rayleigh scattering. Suppose the individual cloud layer has properties (as described in Section 2.2) of τ^c, ω_0^c and x_l^c . Suppose the individual Rayleigh scattering layer has $\tau^R, \omega_0^R = 1.0$ and x_l^R .

The total optical depth, τ^T , is then a sum of the individual layers:

$$\tau^T = \tau^c + \tau^R$$

The total single scatter albedo, ω_0^T is a weighted sum:

$$\omega_0^T = \frac{\omega_0^c \tau^c + \tau^R}{\tau^c + \tau^R}$$

The total phase function moments, x_l^T are a different weighted sum:

$$x_l^T = \frac{\omega_0^c \tau^c x_l^c + \tau^R x_l^R}{\omega_0^c \tau^c + \tau^R}$$

The combined layer is now specified. The same steps are used for an aerosol layer of τ^a, ω_0^a and x_l^a .

(Special thanks to Adam and Don for explaining this approach!)